INDERSCIENCE PUBLISHERS
Linking academia, business and industry through research

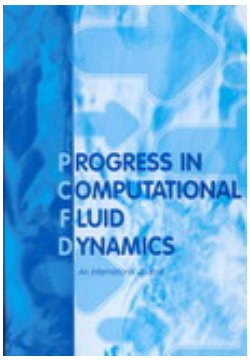

Progress in Computational Fluid Dynamics, An International Journal

ISSN online: 1741-5233 - ISSN print: 1468-4349
https://www.inderscience.com/pcfd

Analysis of flow and thermal characteristics of hybrid nanofluids within a microchannel under magnetic field

Hakan Türker, Elif Büyük Öğüt, Erman Aslan

DOI: 10.1504/PCFD.2024.10065361

Article History:

Received:	14 January 2024
Last revised:	23 March 2024
Accepted:	23 March 2024
Published online:	06 January 2025

Analysis of flow and thermal characteristics of hybrid nanofluids within a microchannel under magnetic field

Hakan Türker

Institute of Sciences,
Kocaeli University,
TR-41380, Kocaeli, Turkey
Email: hkn.turk.er@hotmail.com

Elif Büyük Öğüt and Erman Aslan*

Department of Mechanical Engineering,
Kocaeli University,
TR-41380, Kocaeli, Turkey
Email: elif.ogut@kocael.edu.tr
Email: erman.aslan@kocaeli.edu.tr
*Corresponding author

Abstract: The study investigates the flow and thermal characteristics of microchannels with varying geometries and boundary conditions. Water is used as the base fluid, with Al_2O_3 and CuO nanoparticles as additives. The analysis begins with a straight microchannel, followed by comparisons with sinusoidal or sine wave-shaped channels. Additionally, the effects of a magnetic field on a straight microchannel are explored. The numerical simulations conducted using ANSYS Fluent software, cover Reynolds numbers (Re) of 100, 300, 700, and 1,000 in laminar flow, along with volume fractions of 1%, 2%, 3%, 4%, and 5%. A magnetic field intensity of 0.1T is applied for the magnetohydrodynamic (MHD) effect. The results presented as Nusselt numbers, pressure drop, and thermal performance factor graphs, indicate an increase in Nusselt number with rising Reynolds number and decreasing volume fractions. Pressure drop also rises with increasing Reynolds number and volume fractions.

Keywords: finite volume method; laminar flow; microchannel; nanofluid; magnetohydrodynamics; MHD; convective heat transfer; pressure drop.

Reference to this paper should be made as follows: Türker, H., Öğüt, E.B. and Aslan, E. (2025) 'Analysis of flow and thermal characteristics of hybrid nanofluids within a microchannel under magnetic field', *Progress in Computational Fluid Dynamics*, Vol. 25, No. 1, pp.31–43.

Biographical notes: Hakan Türker received his BSc in Mechanical Engineering from the Balıkesir University and MSc from the Kocaeli University. He is a Quality and Test Engineer at TÜRBOSAN TÜRBOMAKİNALAR SANAYİ VE TİCARET A.Ş. His main research areas are nanofluid, CFD and heat transfer.

Elif Büyük Öğüt graduated from Trakya University with a BS and PhD in Mechanical Engineering. She is currently a Professor in the Mechanical Engineering Department at Kocaeli University. Her research interests include numerical simulation, MHD, natural and mixed convection in enclosure, and nanofluids.

Erman Aslan received his BSc, MSc, and PhD in Mechanical Engineering from the University of Sakarya, Turkey. He was a visiting researcher to prepare his PhD thesis at Duesseldorf University of Applied Sciences, Germany. He is an Associate Professor of Mechanical Engineering Department at Kocaeli University, Turkey. His main research area is Lattice Boltzmann method, computational fluid dynamics, forced convection, aerodynamics, heat transfer and solving PDE with numerical methods.

1 Introduction

In response to research and development efforts in the manufacturing sector, heat exchangers have progressively evolved to microscale dimensions, with channels featuring a hydraulic diameter ranging from 1 to 100 μm being classified as microchannels (Manay et al., 2012). These microscale systems have garnered significant attention in

engineering due to their longer lifespan, reduced weight, and lower cost, offering substantial advantages in both academic literature and practical applications. The popularity of microchannels began to surge in the early 2000s, primarily attributed to their enhanced heat transfer capabilities relative to traditional channels and pipe flows.

In systems involving microfluids, surface effects play a paramount role in flow and heat transfer dynamics. Notably, in systems with a characteristic length of 1m, the surface-to-volume ratio stands at approximately $1m^{-1}$, while in microfluidic systems with a size of 1 μm, this ratio escalates to a staggering $10^{6}m^{-1}$. This remarkable million-fold increase in surface area concerning the device's mass profoundly influences mass, momentum, and energy transfer along these abundant surfaces (Avci, 2008).

Hybrid nanofluids have emerged as a recent development, wherein two or more nanoparticles are meticulously combined to enhance heat transfer properties, distinct from uniform nanoparticles (Huminic, 2020). Several factors, including nanoparticle synthesis, thermal conductivity, nanofluid preparation methods, particle size, nanoparticle compatibility, shape within the fluid, and the establishment of an effective thermal network, have been explored as fundamental parameters affecting heat transfer improvement (Salman et al., 2020).

In general, two fundamental methods for augmenting heat transfer, active and passive, have been recognised (Kuppan, 2020). Passive heat transfer enhancement methods mostly involve geometry modifications on the heat transfer surface (Bhattacharyya et al., 2019) or in the flow domain via inserts along the flow path (Bhattacharyya et al., 2020). In our case, the integration of nanoparticles into the working fluid to boost heat transfer can also be categorised as a passive method. In combination with nanoparticles, a magnetic field can be applied that provides additional means of heat transfer control (Biswas et al., 2022) representing an active approach. This active method is also considered in the present study, entailing the application of a magnetic field to influence the working fluid, which falls under the domain of magnetohydrodynamics (MHD). MHD focuses on the flow of electrically conductive fluids under the influence of a magnetic field, resulting from the amalgamation of the Navier-Stokes equations and the Maxwell equations for the electric field.

This study delves into the impact of nanofluids and hybrid nanofluids in microchannels, with and without MHD effects on convective heat transfer and pressure drop. The literature review is divided into two main categories: studies related to nanofluids and hybrid nanofluids in microchannels, and studies incorporating MHD effects.

The first category explores investigations involving nanofluids and hybrid nanofluids in microchannels. Vinoth and Sachuthananthan (2021) conducted a comparative analysis of heat transfer and flow characteristics in a microchannel heat exchanger employing newly designed pentagonal and triangular fin geometries. In this study, both nanofluids and hybrid nanofluids were employed. The nanofluids used encompassed CuO-Water and Al_2O_3-Water, and an experimental investigation was performed using the Al_2O_3-CuO/Water hybrid nanofluid. Similarly, Krishna et al. (2021) carried out a numerical investigation to evaluate heat transfer and pressure drop characteristics in a circular microchannel heat exchanger, using a hybrid nanofluid as the coolant. The study compared different mass flow rates and volume fractions. Additionally, Ghachem et al. (2021) conducted a numerical analysis of heat transfer in a crossflow micro-heat exchanger featuring rectangular wavy channels and a hybrid nanofluid. The working fluid comprised hot and cold nanofluids flowing through the upper and lower cross channels, respectively. Kumar and Sarkar (2020) performed experimental examinations of the hydrothermal characteristics of Al_2O_3-MWCNT-Water hybrid nanofluid in a minichannel heat exchanger, exploring different Reynolds numbers and inlet temperatures. Moreover, Ekiciler and Çetinkaya (2020) analysed monotype nano-fluid and hybrid nanofluid in a ribbed channel under turbulent flow conditions. They scrutinised Nusselt number, friction factor, temperature contours, and turbulence intensity, along with the significance of geometry, Reynolds number, and nanoparticle types. Further research by Asadi et al. (2020) probed the rheological behaviour and dynamic viscosity of CuO-TiO_2/water hybrid nanofluid, examining the chemical, atomic, and surface structures of the nanoparticles. Goudarzi et al. (2020) conducted a study investigating the effect of nanoparticle motion due to Brownian motion on the natural convection of Ag-MgO/Water hybrid nanofluid. The study was executed on a cavity with sinusoidally oscillating walls. Gravndyan et al. (2017) performed a computational fluid dynamics analysis of laminar flow and heat transfer in a recessed microchannel employing Water-TiO_2 nanofluid as the working fluid. Lastly, Cakir and Aktürk (2022) delved into the thermal performance of nanofluids in a wavy microchannel, investigating Al_2O_3, CuO, Fe_2O_3, TiO_2, and SiO_2 nanoparticles in different volume fractions and Reynolds numbers.

The second category involves investigations of nanofluids and hybrid nanofluids in microchannels with the MHD effect. Aminossadati et al. (2021) conducted a numerical analysis of laminar forced convection in a horzontal microchannel using a Water-Al_2O_3 nanofluid. Their study revealed increased thermal performance at high Reynolds and Hartmann numbers, with solid volume fraction playing a significant role in enhancing the Nusselt number. Shiriny et al. (2019) examined forced convection heat transfer in a microchannel with rectangular geometry featuring triangular protrusions, with the application of a magnetic field. Higher Reynolds numbers and stronger magnetic fields led to increased heat transfer, emphasising the importance of nanoparticle volume fraction. Sivasankaran and Narrein (2020) explored the effects of a magnetic field on heat transfer and fluid flow in a trapezoidal microchannel heat exchanger. Their study highlighted the role of channel dimensions and magnetic fields in influencing Nusselt numbers and improving heat transfer. Ma et al. (2019) performed a numerical analysis on

the effects of a magnetic field on forced convection and heat transfer in a hybrid nanofluid containing Ag-MgO/Water. The results indicated enhanced heat transfer at the junction of the heater and cooler, particularly near sharp corners. Additionally, magnetic field application significantly impacted heat transfer. Nguyen et al. (2020) investigated the effects of a magnetic field on heat transfer and entropy production in a microchannel with triangular ribbed walls. They found that magnetic fields reduced vortex intensity and enhanced heat transfer, with a simultaneous increase in entropy generation. Soltanipour et al. (2017) conducted a numerical analysis to explore forced convection and entropy production in an Al_2O_3-Water nanofluid in a microchannel. Their study emphasised the significance of position-dependent magnetic fields, which induced vortices and varied significantly with Hartmann numbers. In addition to these, the natural convection problem with the MHD effect in a closed enclosure has been studied by Selimefendigil et al. (2014). Selimefendigil and Öztop (2023) investigated the effects of combining the use of a magnetic field with rotating cylinders on thermal processes and phase transitions in a T-shaped branching channel.

This study focuses on conducting numerical investigations into the flow and thermal characteristics of microchannels featuring various geometries and boundary conditions. Water serves as the base fluid, while Al_2O_3 and CuO nanoparticles are introduced as additives. Initially, the study examines flow within a straight microchannel. Subsequently, a comparative analysis is performed by introducing sinusoidal or sine wave-shaped geometric slopes to the straight microchannel. Furthermore, the study explores the flow and thermal behaviours when a magnetic field is applied to the straight microchannel. The numerical simulations are executed using the finite volume method-based commercial software ANSYS Fluent (2018). Within the scope of this study, different Reynolds numbers (Re = 100, 300, 700, and 1,000) are investigated under laminar flow conditions, alongside various volume fractions (1%, 2%, 3%, 4%, 5%). A magnetic field intensity of 0.1T is applied to account for the MHD effect. The findings are presented in the form of Nusselt number, heat transfer coefficient, and pressure drop graphs across the range of Reynolds numbers.

2 Methodology

2.1 Geometry

A geometry of straight and wavy microchannels is developed using CAD program. Quantitative geometrical properties are represented in Table 1, where D_h is hydraulic diameter, H is height, W is width, L is length. Pitch (R), inlet length (L_i) and exit length (L_e) is for wavy channel. The geometry of

a straight

b wavy channels are shown in Figure 1.

Table 1 Geometrical parameters of channel

Dh (μm)	*H* (μm)	*W* (μm)	*L* (mm)	*R* (mm)	L_i (mm)	L_e (mm)
100	100	100	40	6.28	4.71	3.87

Figure 1 Geometry of (a) straight and (b) wavy channel

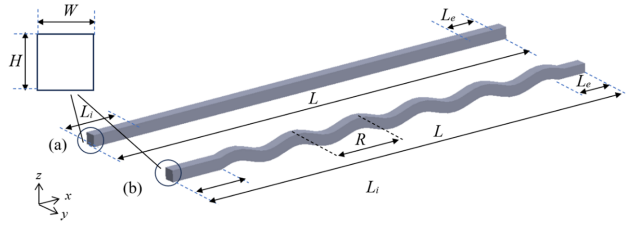

2.2 Governing equations

In our present study, water has been used as the base fluid, while Al_2O_3 and CuO nanoparticles have been used as additives. The mean free path of base fluid (water) is 0.278 ηm, and hydraulic diameter is of both channel is 100 μm (see in Table 1), according to these variables our Knudsen number is 2.78×10^{-6}, therefore we can use continuum approach. The fluid flow and heat transfer are governed through continuity, momentum and energy equations (1)–(3) (Ebrahimi et al., 2016; Cengel and Cimbala, 2010).

$$\nabla \cdot U = 0 \tag{1}$$

$$\nabla \cdot U(U) = -\frac{1}{\rho}\nabla p + \nabla \cdot (v \cdot \nabla U) \tag{2}$$

$$\nabla \cdot U\left(\rho C_p T_f\right) = \nabla \cdot \left(k_f \cdot \nabla T_f\right) \tag{3}$$

where ρ is density of the fluid, U is velocity, μ represents the dynamic viscosity, k_f is the thermal conductivity of the fluid, T_f represents the fluid temperature and C_p is the specific heat. The equation for momentum under the influence of a magnetic field.

2.3 Numerical setup and boundary conditions

The governing equations can be discretised by a variety of procedures, including the finite volume (Xia et al., 1997), finite element (Benim and Zinser, 1986; Benim, 1990), and the Lattice Boltzmann (Aslan et al., 2012) methods. Although the latter is also frequently used in mini and micro-channels (Chen et al., 2022), the finite volume method is preferred in the present study. Thus, the numerical analysis is performed using finite volume method-based commercial software ANSYS Fluent (2018). The flow is considered incompressible, steady-state and laminar. SIMPLE algorithm is used for pressure velocity coupling with second-order upwind discretisation schemes to compute numerically. Default under-relaxation factors, for pressure, momentum, and energy, were applied as 0.3, 0.7 and 1.0, respectively. As the convergence criteria, a residual value 10^{-6}, is required for all equations except

energy equation. The residual value for energy equation was used as 10^{-8}. Three-dimensional structural meshes have been used in both straight microchannels and wavy microchannels In Figure 2, the mesh structure for the straight microchannel is shown in (a) front and (b) profile views. As depicted in Figure 2, a finer mesh structure is utilised in regions closer to the wall, while a coarser mesh structure is employed in regions farther away from the wall.

In present study, two geometric configurations which are straight and wavy channels are used. We consider three cases, which are straight microchannel with hybrid nanoparticles, wavy microchannel with hybrid nanoparticles, and straight microchannels with hybrid nanoparticles and MHD. First, the effect of geometry on heat transfer and flow will be examined in hybrid nanoparticle microchannels. Then, the effect of MHD on heat transfer and flow will be investigated in a straight microchannel. The used boundary conditions of three cases are listed in Table 2. At the, constant temperature is applied for energy equation, and constant velocity is determined for momentum equation. The inlet velocities change of course for considered four Reynold numbers (Re = 100, 300, 700 and 1,000). At the outlet, pressure outlet boundary condition is applied which is zero-gauge pressure and zero temperature gradient for momentum and energy equation, respectively. Bottom surface is heated with constant heat flux. Top and side surfaces are adiabatic. The no-slip boundary conditions are applied all surfaces. Only for MHD case, 0.1 of magnetic heat flux density is applied at top surface.

2.4 Thermophysical properties and parametric definition

Water has been employed as the base fluid, and nanoparticles of Al_2O_3 and CuO have been used as additives. Both of nanoparticles added in equal amounts to base fluid (water) The thermophysical properties of water, Al_2O_3 and CuO are listed in Table 3 (Vajjhai et al., 2010; Sheikholeslami et al., 2014; Ahmed et al., 2021).

Figure 2 Mesh structure for straight microchannel (a) front and (b) profile views

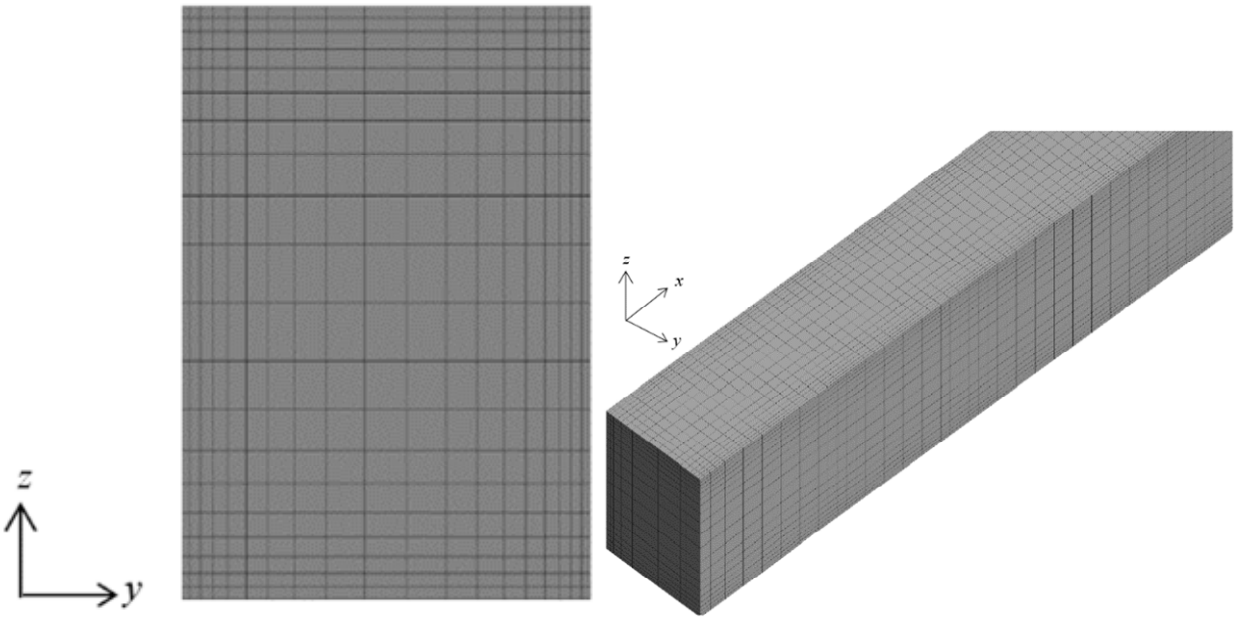

(a) (b)

Table 2 Boundary condition of three cases

	Boundary conditions				
Geometrical position of microchannel	*Temperature [°C]*	*Velocity [m/s]*	*Pressure [Pa]*	*Heat flux [W/m²]*	*Magnetic flux density [Tesla]*
Inlet	25				
-	-	-			
Outlet	-	-	Pgauge = 0	-	-
Bottom surface	-	0	-	1,000	-
Top surface	-	0	-	0 (adiabatic)	0.1
Side surfaces	-	0	-	0 (adiabatic)	-

Table 3 Thermophysical properties of water, Al_2O_3 and CuO

	ρ [kg/m³]	C_p [J/kgK]	k [W/mK]	μ [kg/m.s]	σ [Ω.m]$^{-1}$
Water	997.1	4,189	0.613	8.91×10^{-4}	0.05
Al2O3	3,600	765	36	-	10^{-12}
CuO	6,500	533	17.65	-	10^{-10}

In the context of this study, it is assumed that the single phase nanofluids used are homogeneously distributed in water, and the working fluid will be considered as a single phase. The following equations are used to determine the thermophysical properties of the hybrid nanofluid (Behroyan et al., 2015; Aminian et al., 2020). The effective density of liquids has been.

$$\rho_{hnf} = (1-\varphi)\rho_f + \varphi\rho_{np} \tag{4}$$

In equation (4), the density of hybrid nanofluid (ρ_{nf}) is acquired, where φ is total volume fraction, ρ_f is density of base fluid and ρ_{np} is density of hybrid nanoparticles. Specific heat of hybrid nanofluids ($C_{p,hnf}$) is calculated as;

$$C_{p,hnf} = (1-\varphi)C_{p,f} + \varphi C_{p,np} \tag{5}$$

where $C_{p,f}$ is specific heat of base fluid, and $C_{p,np}$ represents specific heat of nanoparticles. Viscosity is determined using Brinkmann model.

$$\mu_{hnf} = \mu_f / (1-\varphi)^{2.5} \tag{6}$$

where μ_{nf} is dynamic viscosity of hybrid nanofluid and μ_f exhibits dynamic viscosity of base fluid. Thermal conductivity is calculated as using correlation of Yu and Choi (2003).

$$k_{hnf} = \frac{k_{np} + (n-1)k_f - (n-1)(k_f - k_{np})\varphi}{k_{np} + (n-1)k_f + (k_f - k_{np})\varphi} k_f \tag{7}$$

where k_{nf} represents conductivity of hybrid nanofluids, k_{np} is conductivity of hybrid nanoparticles, n is shape factor and k_f is thermal conductivity of base fluid. Electrical conductivity of hybrid nanofluid ($\sigma_{e,hnf}$) is computed as

$$\sigma_{e,hnf} = (1-\varphi)\sigma_{e,f} + \varphi\sigma_{e,np} \tag{8}$$

where $\sigma_{e,f}$ and $\sigma_{e,np}$ are electrical conductivity of base fluid and electrical conductivity of nanoparticles, respectively.

The properties determined by equations (4)–(8) for Al_2O_3 and CuO are expressed using the following equations.

$$\varphi = \varphi_{Al_2O_3} + \varphi_{CuO} \tag{9}$$

$$\rho_{np} = \left(\varphi_{Al_2O_3}\rho_{Al_2O_3} + \varphi_{CuO}\rho_{CuO}\right)/\varphi \tag{10}$$

$$k_{np} = \left(\varphi_{Al_2O_3}k_{Al_2O_3} + \varphi_{CuO}k_{CuO}\right)/\varphi \tag{11}$$

$$C_{p,np} = \left(\varphi_{Al_2O_3}C_{p,Al_2O_3} + \varphi_{CuO}C_{p,CuO}\right)/\varphi \tag{12}$$

$$\sigma_{e,np} = \left(\varphi_{Al_2O_3}\sigma_{e,Al_2O_3} + \varphi_{CuO}\sigma_{e,CuO}\right)/\varphi \tag{13}$$

And thermophysical properties of Al_2O_3-CuO hybrid nanoparticles are listed Table 4.

The use of higher volume fractions in nanofluids leads to serious problems such as sedimentation, erosion and higher pressure drop, etc. (Tawfik, 2017; Kleinstreuer and Feng, 2011). Therefore, in our own study, five volume fractions were utilised, in the order of 1%, 2%, 3%, 4%, and 5%.

For evaluating convective heat transfer, convective heat transfer coefficient (h) is calculated as

$$h = Q \Big/ \left(T_w - \frac{T_i + T_e}{2}\right) \tag{14}$$

where Q is heat flux, T_w, T_i and T_e represent wall temperature, inlet temperature and exit temperature of the microchannel, respectively. Nusselt number (Nu) can be calculated via convective heat transfer coefficient, thermal conductivity of fluid (k) and hydraulic diameter (D_h).

$$Nu = hD_h/k \tag{15}$$

Reynolds number is based on inlet velocity and hydraulic diameter (see in Table 2). The friction factor is defined as

$$f = \left(\left(\Delta P/L\right)D_h\right)/2\rho u^2 \tag{16}$$

where pressure differences (ΔP) is calculated with using outlet (P_o) and inlet (P_i) pressures of microchannel

$$\Delta P = P_o - P_i \tag{17}$$

In order to evaluate convective heat transfer and friction factor together, thermal performance factor (γ) is determined. It compares the cases between base fluid and hybrid nanofluids and it is calculated as

$$\gamma = \left(Nu/Nu_{bf}\right)/\left(f/f_{bf}\right)^{1/3} \tag{18}$$

where Nu_{bf} and Nu represent the Nusselt number of base fluid and Nusselt number of hybrid nanofluid, with the same manner f_{bf} and f exhibit the friction factor of base fluid and friction factor of hybrid nanofluid.

Table 4 Thermophysical properties of Al_2O_3-CuO hybrid nanoparticles

	φ = 1%	φ = 2%	φ = 3%	φ = 4%	φ = 5%
ρ [kg/m³]	1,037.629	1,078.158	1,118.687	1,159.216	1,199.745
Cp [J/kgK]	4,007.199	3,848.315	3,700.944	3,563.877	3,436.071
k [W/mK]	0.6303	0.6480	0.6660	0.6844	0.7031
μ [kg/m.s]	0.0009136	0.0009371	0.00009614	0.0009867	0.0010129
σ [Ω.m]$^{-1}$	0.0495	0.0490	0.0485	0.0480	0.0475

2.5 Validation

In order to validate our numerical procedure, one validation case is determined. Validation case based on the experimental investigation of the Nusselt number and friction characteristics straight microchannels using de-ionised water (Chen et al., 2014). The aspect ratio and hydraulic diameter of the straight microchannel used in the experiment is 2.5 and 160 μm, respectively. The experiments were conducted within the range of Reynolds numbers between 350 and 1,500. In order to validate this experimental study numerically, we relied on the study of Khan et al (2021). They adopted the physical properties of the de-ionised water from the studies conducted by Okhotin et al. (1972) and Ebrahimi et al (2015). The solver setting in this numerical study have been applied in our own work.

Figure 3 Validation of numerical model (a) for Nusselt number and (b) friction factor

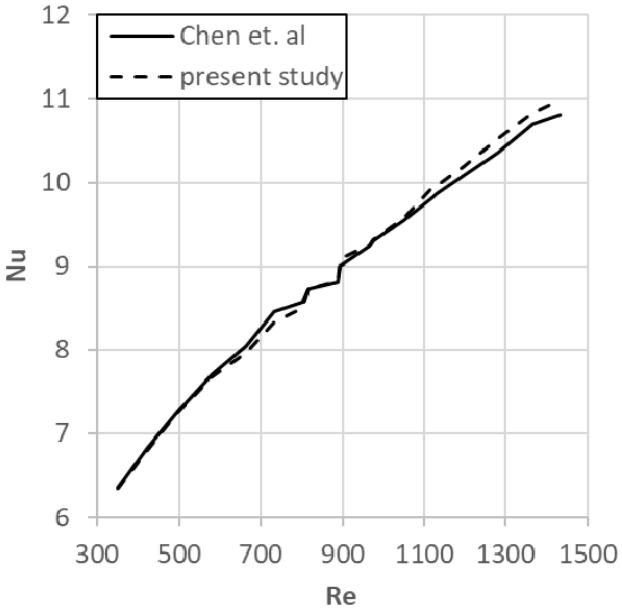

(a)

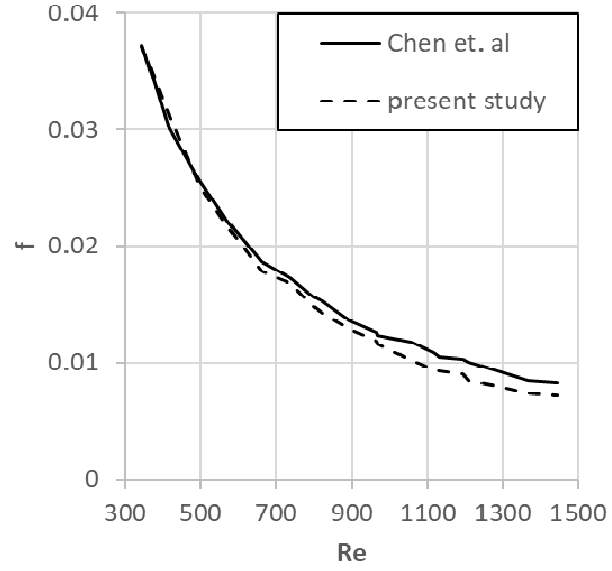

(b)

Figure 3 shows the results of the validation study for Nusselt number and friction factor. According to Figure 3, it is observed that at low Reynolds numbers, both the experimental and numerical results of both the Nusselt number and friction factor align closely. However, as the Reynolds number increases, slight differences emerge between experimental and numerical results. At the highest Reynolds number, the relative true error is approximately 12% for the Nusselt number, while this value is 1% for the friction factor. We observe that the numerical study is validated within these relative true errors.

2.6 Grid independence study

Grid independency study of Nusselt number and pressure drop is done for straight and wavy microchannel without MHD effect at Re = 1,000 and for Al_2O_3-CuO/Water, volume fraction of %5. Figure 4 presents the grid independency. In straight and wavy microchannel, we determined seven grid densities, and densities are obtained using the same sized finite elements. According to Figure 4, nearly one million mesh numbers are determined as a grid independent mesh number for straight (1014220) and wavy microchannels (938400).

Figure 4 Grid independence study

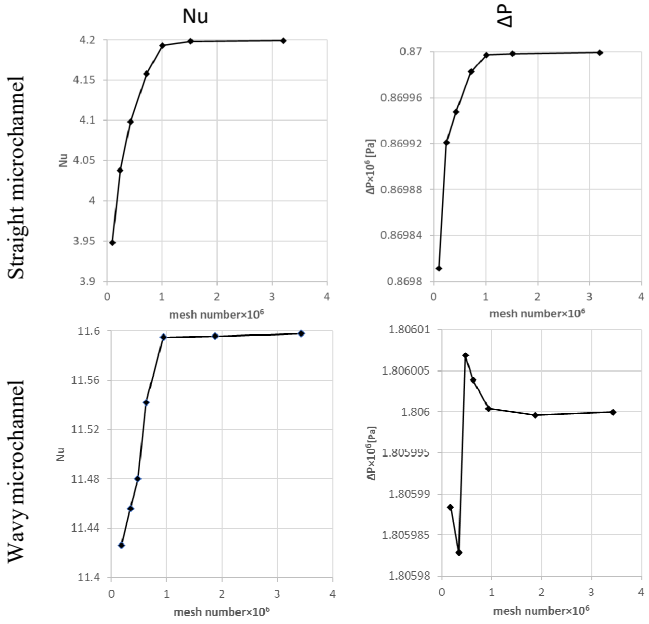

3 Results and discussion

3.1 Straight microchannel

Figure 5 represents the velocity distribution of straight microchannel in the middle section of the inlet length (L_i) for (a) φ = 0%, (b) φ = 1% and (c) φ = 5% at Re = 100. Within the inlet length, flow reaches the fully developed conditions. With an increase in volume fraction, the velocity value consistently decreases. As one can observed at Table 4, addition of nanoparticles increases the density and

viscosity of the hybrid nanofluid. The increase density due to the addition of Al_2O_3-CuO nanoparticles to water absorbs the increase in viscosity and becomes dominant. Therefore, increasing nanoparticles penetration in to the base fluid (water), leads to decrease in velocity at a constant Reynolds number, as clearly demonstrated in the Figure 4.

Figure 5 velocity distribution of straight microchannel in the middle section of the inlet length (L_i) for (a) φ = 0%, (b) φ = 1% and (c) φ = 5% at Re = 100 (see online version for colours)

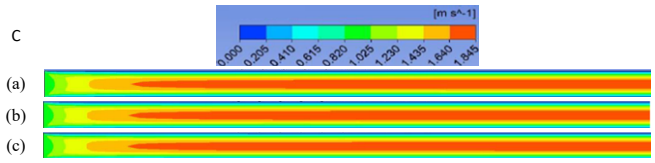

Figure 6 shows the temperature distribution of straight microchannel in the middle section of the inlet length (L_i) for (a) φ = 0%, (b) φ = 1% and (c) φ = 5% at Re = 100. It is observed that, at a constant Reynolds number (Re = 100), as the volume fraction increases, the temperature of lower surface, where a constant heat flux is applied, slightly increases as one progress towards the outlet region of the microchannel

Figure 6 Temperature distribution of straight microchannel in the middle section of the inlet length (L_i) for (a) φ = 0%, (b) φ = 1% and (c) φ = 5% at Re = 100 (see online version for colours)

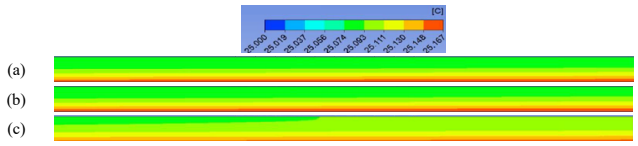

Figure 7 exhibits the Nusselt number variation with Reynolds number for straight microchannel. As the Reynolds number leads to an increase in Nusselt number, while an increase in volume fraction results in a decrease in Nusselt number. The maximum Nusselt number is acquired for water. Nusselt number is 2.95 and for water at Re = 100. In the case, where the volume fraction is 5%, Nu is 2.91 for the Al_2O_3-CuO/Water hybrid nanofluid at Re = 100. At Re=1000, Nusselt numbers are 4.47 and 4.42 for water and Al2O3-CuO/Water hybrid nanofluid with volume fraction of 5%. When comparing water at Re = 100 with addition of 5% nanoparticles, there is a decrease of approximately 1.35% in the Nusselt number value. For a Reynolds number of 1000, this reduction in the Nusselt number is 5.59%. The decrease in the Nusselt number is attributed to the increase in the thermal conductivity (see in Table 4) of the fluid due to addition of nanoparticles to water.

Figure 8 represents the pressure drop variations with Reynolds number for straight microchannel. Pressure drop increases with Reynolds number as expected. An increase in nanoparticle volume fraction within the base fluid leads to an increase in pressure drop, and the reason for this the rise in viscosity (see in Table 4). At Re = 100, pressure drop is enhanced as 6.84% with addition of hybrid nanoparticles to the base fluid, while at Re = 1,000, this value is calculated as 6.96%.

Figure 7 Nusselt number variation with Reynolds number for straight microchannel

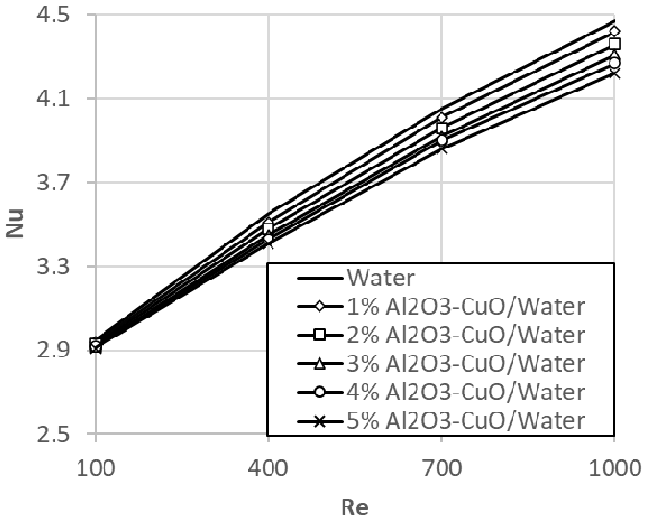

Figure 8 Pressure drop variation with Reynolds number for straight microchannel

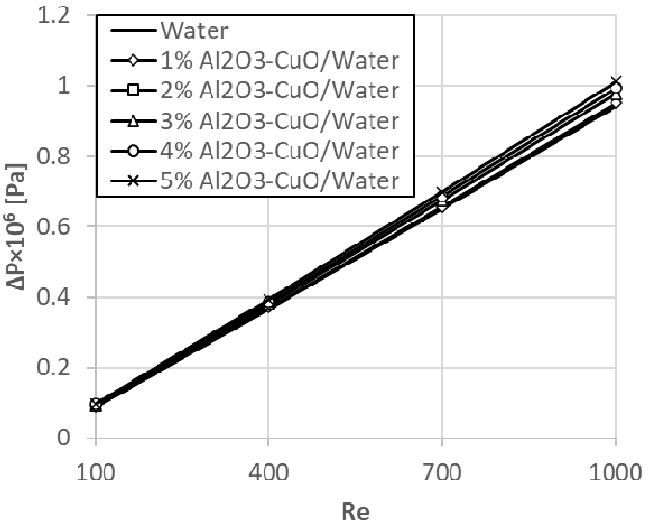

Thermal performance factor variation with Reynolds number is shown in Figure 9 for straight microchannel. Figure 9 consists only two volume factions which are 1% and 5%. Thermal performance factor decreases with Reynolds number. As one can observed that, with increase of volume fractions, thermal performance factor leads to decrease, due to the increases pressure drop caused by the addition of nanoparticles to the base fluid.

3.2 Wavy microchannel

Figure 10 represents the velocity distribution of wavy microchannel in the middle section of the inlet length (L_i) for (a) φ = 0%, (b) φ = 1% and (c) φ = 5% at Re = 100. The same observations and comments as in Figure 5 can be made for Figure 10. Furthermore, when examining equivalent volume fractions, the velocity values in the wavy

microchannel are very close to the velocity values in the straight microchannel.

Figure 9 Thermal performance factor variation with Reynolds number for straight microchannel

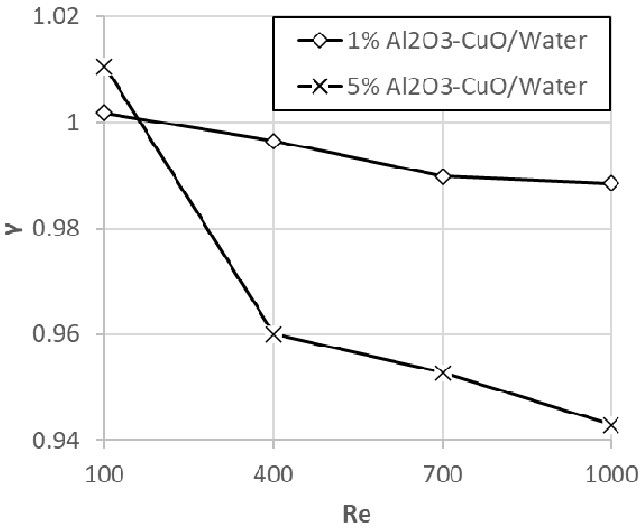

Figure 10 Velocity distribution of wavy microchannel in the middle section of the inlet length (L_i) for (a) φ = 0%, (b) φ = 1% and (c) φ = 5% at Re = 100 (see online version for colours)

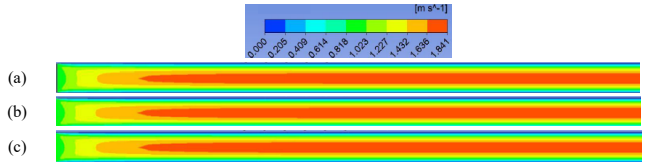

Temperature distribution of the wavy microchannel in the middle section of the inlet length (L_i) is shown in Figure 11 for (a) φ = 0%, (b) φ = 1% and (c) φ = 5% at Re = 100. The same comments as those in Figure 6 can also be made for Figure 11. Additionally, the temperature values in the wavy microchannel are so close to the temperature values in straight microchannel when equivalent volume fractions are considered.

Figure 11 Temperature distribution of wavy microchannel in the middle section of the inlet length (L_i) for (a) φ = 0%, (b) φ = 1% and (c) φ = 5% at Re = 100

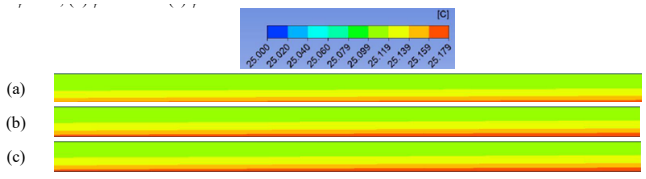

Figure 12 shows the Nusselt number variation with Reynolds number for wavy microchannel. The relation between the Nusselt number, Reynolds number and volume fractions is akin that in the straight channel, therefore, the observations and comments in Figure 7 can also be applied to Figure 12. For only base fluid (water), Nusselt number is calculated as 4.4 at Re = 100. Nusselt number is computed as 4.13 for Al_2O_3-CuO/Water hybrid nanofluid in the case where volume fraction is 5% at Re = 100. With the same manner, at Re = 1,000, Nusselt numbers are 12.54 and 11.29 for water and Al_2O_3-CuO/Water hybrid nanofluid with volume fraction of 5%. When comparing water with the addition of 5% nanoparticles at Re = 100, there is a decrease of approximately 6.13% in the Nusselt number value. For Re = 1,000, this reduction in the Nusselt number is 9.96%. The reduction in the Nusselt number can be explained by the enhances thermal conductivity, as indicated in Table 4, resulting from the introduction of nanoparticles in to the water.

Figure 12 Nusselt number variation with Reynolds number for wavy microchannel

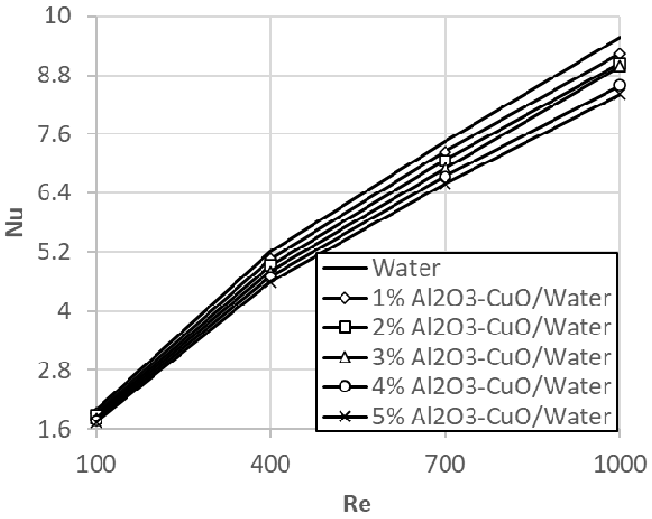

Figure 13 Pressure drop variation with Reynolds number for wavy microchannel

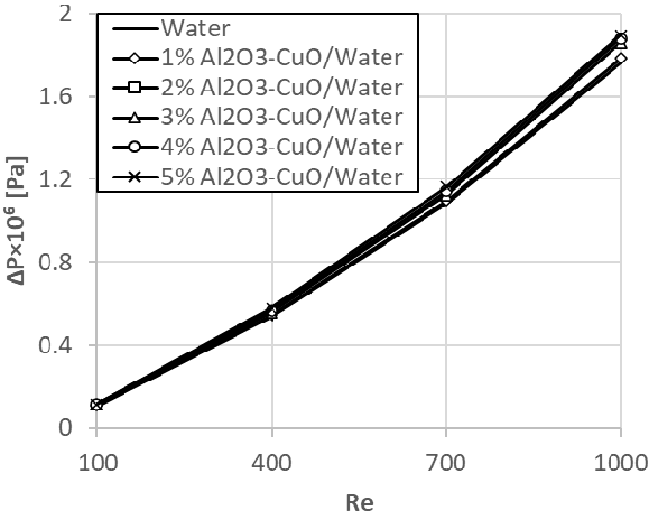

Pressure drop variations according to Reynolds number for wavy microchannel is represented in Figure 13. The relation between pressure drop, Reynolds number and volume fractions resembles that observed in the straight channel. Consequently, the insights and interpretations in Figure 8 are applicable to Figure 13 as well. At Re = 100 and Re = 1,000, pressure drop increases as 6.89% with addition p_f hybrid nanoparticles to the base fluid.

Figure 14 Thermal performance factor variation with Reynolds number for wavy microchannel

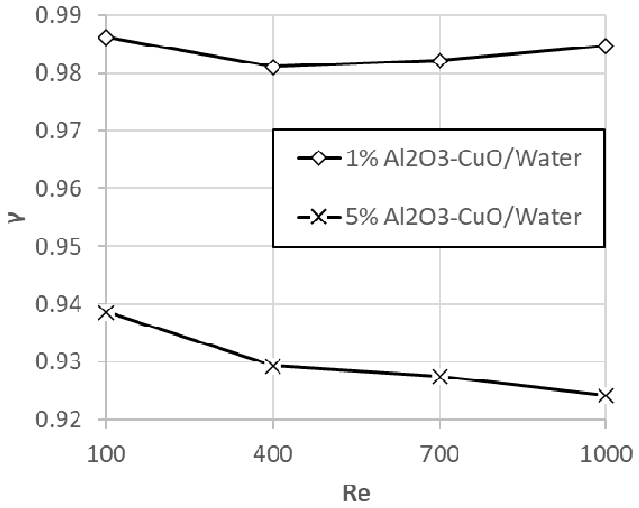

Figure 14 shows the thermal performance factor variation with Reynolds number of wavy microchannel for only two volume fractions which are 1% and 5%. Thermal performance factor decreases with Reynolds number for volume fraction of 5%, however it generally stays constant for volume fraction of 1%. The comments regarding the decrease in thermal performance factor with respect to volume fractions are applicable within the wavy microchannel and similar observations can be made in the straight microchannel.

3.3 Straight microchannel with MHD

Figure 15 exhibits the velocity distribution of straight microchannel with MHD in the middle section of the exit length (L_e) for (a) φ = 0%, (b) φ = 1% and (c) φ = 5% at Re = 100. Firstly, the comments and observations from Figure 5 and Figure 10 can be extended to Figure 15. However, the physics of the flow in the MHD affected straight microchannel undergoes some slight alternation, especially at the beginning of the inlet. In the straight channel with only the nanofluid applied (Figure 5), flow enters the straight microchannel uniformly, later it evolves into a fully developed flow. Here, the uniform flow is slightly distributed after entering the straight microchannel, but eventually reaches a fully developed state. Additionally, the impact of MHD results in velocity reductions compared to the previous straight microchannel configuration.

Temperature distribution of straight microchannel with MHD in the middle section of the exit length is exhibits in Figure 16 for (a) φ = 0%, (b) φ = 1% and (c) φ = 5% at Re = 100. Initially, the akin comments and observations from Figure 6 and Figure 11 can be done to Figure 16. In the MHD affected straight microchannel, the temperature increase caused by heat flux at the bottom walls also effects the upper side of microchannel. This is in contrast to the straight channel without MHD effects. Thus, we can assert that straight microchannel with MHD generates higher transfer than straight microchannel without MHD.

Figure 15 Velocity distribution of straight microchannel with mhd in the middle section of the exit length (L_e) for (a) φ = 0%, (b) φ = 1% and (c) φ = 5% at Re = 100 (see online version for colours)

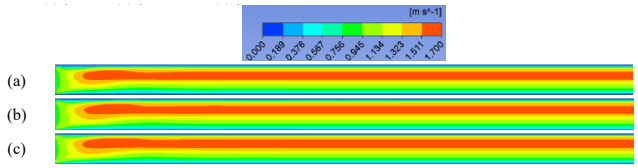

Figure 16 Temperature distribution of straight microchannel with mhd in the middle section of the exit length (L_e) for (a) φ = 0%, (b) φ = 1% and (c) φ = 5% at Re = 100 (see online version for colours)

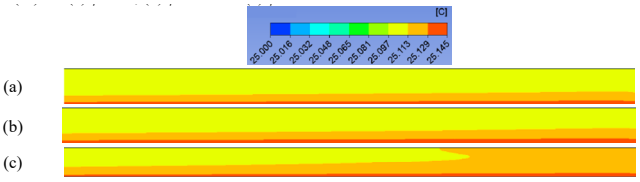

Figure 17 Nusselt number variation with Reynolds number for straight microchannel with MHD

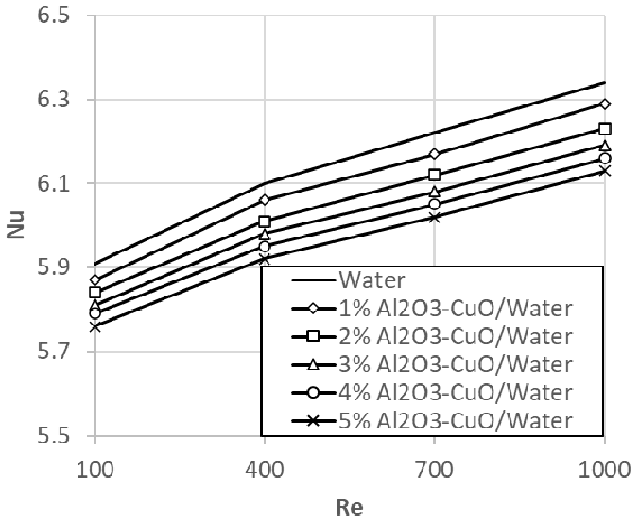

Figure 17 represents the Nusselt number variation with Reynolds number for straight microchannel with MHD. The relationship between the Nusselt number, Reynolds number and volume fractions closely resembles that observed in the straight and wavy microchannels. Consequently, the findings and discussions in Figure 7 and Figure 12 are equally applicable to Figure 17. For the base fluid (water) alone, Nusselt number of 5.91 is obtained at Re = 100. In the case of 5% volume fraction of Al_2O_3-CuO/Water hybrid nanofluid at Re = 100, Nusselt number is estimated as 5.76. Comparing water with the addition of 5% nanoparticles at Re = 1,000 results in a decrease of approximately 2.53% in the Nusselt number value. Likewise, at Re = 1,000, the Nusselt numbers are 6.34 for water and 6.14 for Al_2O_3-CuO/Water hybrid nanofluid. For Re = 1,000, this reduction in the Nusselt number is 3.31%. Again, the decrease in the Nusselt number can be attributed to enhanced thermal conductivity, as indicated in Table 4, arising from the introduction of nanoparticles into the water.

Figure 18 illustrates the pressure drop variations with Reynolds number for straight microchannel with MHD. The relation between pressure drop, Reynolds number and volume fractions mirror the observation made in the straight and wavy microchannels. Therefore, the comments and observations drawn from Figure 8 and Figure 13 can be extended to Figure 18. At Re = 100, the pressure drop increases by 5.9% when hybrid nanoparticles are added to base fluid (water), and for Re = 1,000, this value is determined as 5.85%.

Figure 18 Pressure drop variation with Reynolds number for straight microchannel with MHD

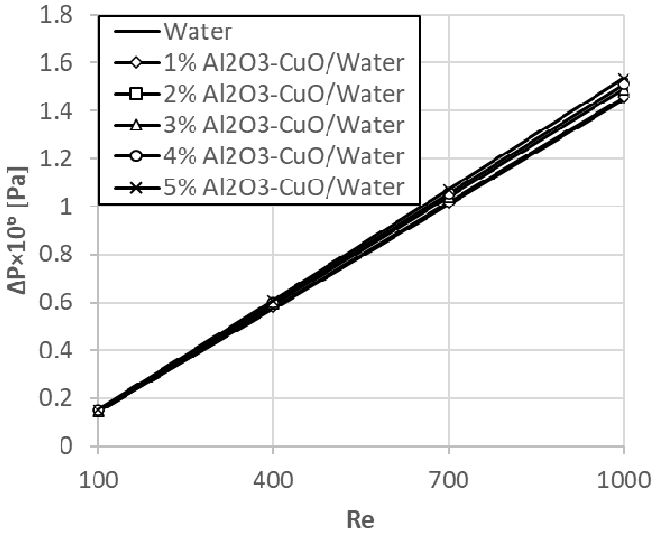

Figure 19 Thermal performance factor variation with Reynolds number for straight microchannel with MHD

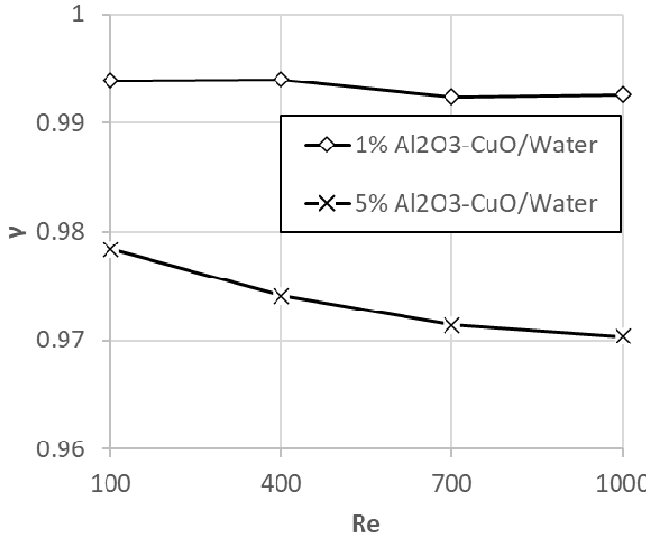

Thermal performance factor variation with Reynolds number in straight microchannel with MHD is depicted in Figure 19 for two specific volume fractions which are 1% and %5. For the volume fraction of 5%, the thermal performance factor decreases with Reynolds number, while it generally remains constant for the volume fraction of 1%. Comments about the decrease in thermal performance based on volume fractions are applicable within the MHD affected straight channel, and the same comments can be made for both straight and wavy microchannels.

3.4 Comparison

Three figures and three tables have been added to collectively compare the effects of microchannel geometry, MHD and the addition of nanoparticle to the base fluid on Nusselt number, pressure drop, and thermal performance. In the comparisons of Nusselt number and pressure drop, results from the base fluid with 5% nanoparticle addition to base fluid are compared between straight microchannel, wavy microchannel and straight microchannel with MHD. For the thermal performance comparison, results with 1% and 5% nanoparticles additions are compared among straight microchannel, wavy microchannel and MHD affected straight microchannel.

Figure 20 Nusselt number comparison

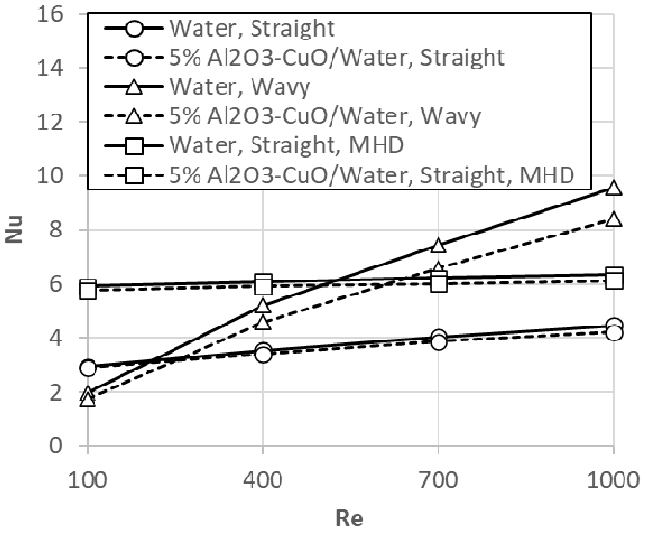

Firstly, Figure 20 represents the Nusselt number comparison. In all cases, Nusselt number increases with Reynolds number, however the rate of increases is highest in the wavy microchannel. Except at Re = 100 and Re = 400, the wavy microchannel consistently yields the highest Number in all cases. The MHD affected straight microchannel has produced higher Nusselt number compared to the straight microchannel. The wavy microchannel has generated higher Nusselt number to straight microchannel. This is attributed to both the effect of MHD and wavy surfaces that enhance mixing and create greater temperature gradients within the flow. At low Reynolds numbers, there is not much differences in the Nusselt numbers produces by the base fluid and the nanoparticle-laden fluid. However, as the Reynolds number increases, the base fluid has produces a higher Nusselt number compared to the flid with added nanoparticles. Additionally, straight channels without MHD effects (Figure 5) have generated higher velocities compared to straight channels with MHD effects (Figure 15). However, in straight channels with MHD effects, velocities are not uniform along the channel, unlike those without MHD

effects. The disruption of uniformity in velocity distribution also affects the temperature distribution (Figure 6 and 14). The temperature distribution, which is less uniform under the MHD effect, results in a higher Nusselt number.

To make a better comparison, the Nusselt number values in Figure 20 are presented in tabular form in Table 5. Comments made in Figure 20 can be referred to within Table 5.

Table 5 Comparison of Nusselt number in tabular form

Re	*Water, straight*	*5% Al_2O_3-CuO/water, straight*	*Water, wavy*	*5% Al_2O_3-CuO/ water, wavy*	*Water, straight, MHD*	*5% Al_2O_3-CuO/water, straight, MHD*
100	2.95	2.91	1.98	1.74	5.91	5.76
400	3.55	3.41	5.20	4.59	6.10	5.92
700	4.05	3.86	7.45	6.69	6.22	6.02
1,000	4.47	4.22	9.57	8.41	6.34	6.13

Figure 21 Pressure drop comparison

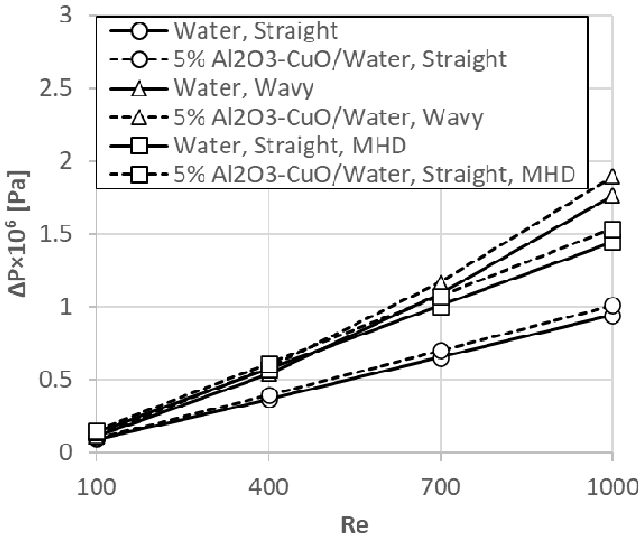

Table 6 Comparison of pressure drop in tabular form

Re	*Water, straight*	*5% Al_2O_3-CuO/ water, straight*	*Water, wavy*	*5% Al_2O_3-CuO/ water, wavy*	*Water, straight, MHD*	*5% Al_2O_3-CuO/ water, straight, MHD*
100	0.090	0.097	0.108	0.117	0.142	0.151
400	0.366	0.393	0.538	0.578	0.573	0.609
700	0.649	0.698	1.085	1.165	1.008	1.070
1,000	0.940	1.011	1.764	1.895	1.445	1.535

Pressure drop comparison is shown in Figure 21. Pressure drop values increase with Reynolds number in all cases. At lowest Reynolds number (Re = 100), all pressure drop values are relatively close to each other. As the Reynolds number increases, the pressure drop values between the cases start to differ. The wavy microchannel generates the highest pressure drop, while the straight microchannel produces the lowest pressure drop, as seen in Figure 20, consistent with the Nusselt numbers.

Figure 22 Thermal performance comparison between base fluid cases and nanofluid cases at varying Reynolds numbers

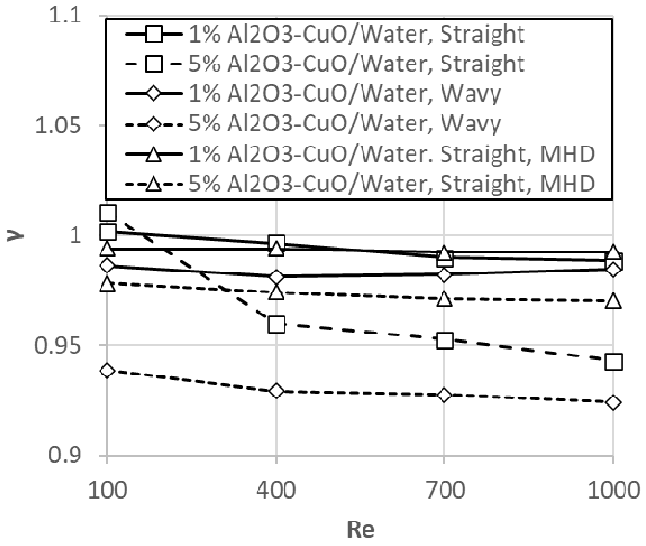

Figure 22 exhibits the thermal performance factor. Generally, thermal performance factor decreases with Reynolds number. The highest thermal performance value was observed at Re = 1,000 for the fluid with 5% added nanoparticles, which is an exception, because in all other cases, the base fluid 1% added nanoparticles produced higher thermal performance. In cases with 1% added nanoparticles, the straight microchannel and MHD affected straight microchannel generally exhibits equivalent thermal performance, while wavy microchannel yields lower thermal performance. In the cases with 5% added nanoparticles to base fluid, the straight microchannel with MHD produces the highest thermal performance, while wavy channel exhibited the lower thermal performance.

To enable a better comparison, the performance values in Figure 22 are presented in tabular form in Table 7. Comments made in Figure 22 can be applied to Table 7.

Table 7 Comparison of thermal performance in tabular form

Re	*1% Al_2O_3-CuO/ water, straight*	*5% Al_2O_3-CuO/ water, straight*	*1% Al_2O_3-CuO/ water, wavy*	*5% Al_2O_3-CuO/ water, wavy*	*1% Al_2O_3-CuO/ water, straight, MHD*	*5% Al_2O_3-CuO/ water, straight, MHD*
100	1.0017	1.0106	0.9862	0.9386	0.9939	0.9784
400	0.9965	0.9600	0.9811	0.9293	0.9940	0.9741
700	0.9898	0.9528	0.9822	0.9275	0.9924	0.9714
1,000	0.9885	0.9429	0.9847	0.9242	0.9926	0.9704

4 Conclusions

The flow and thermal characteristics of straight microchannel, wavy microchannel and straight microchannel with MHD have been numerically examined.

Water has been used as the base fluid, while nanoparticles of Al2O3 and CuO have been added as additives with various volume fractions of 1%, 2%, 3%, 4% and 5%. The finite volume based commercial code ANSYS Fluent (2018) is used in numerical computations. Our numerical formulation is validated with experimental results (Nusselt number and friction factor) in the literature. Numerical studies are carried out in laminar flow regime (Re = 100, 300, 700 and 1,000). A magnetic fluid intensity of 0.1T is used as the MHD effect. The following conclusions can be obtained as below:

- Increasing the Reynolds number leads to an increase in the Nusselt number, while an increase in volume fraction causes a decrease in the Nusselt number, which is attributed to the enhancement of thermal conductivity in hybrid nanofluids as the volume fraction increases
- Pressure drop increases with Reynolds number and volume fractions. The reason for the increase in pressure drop with volume fractions is due to the increase in the viscosity of the hybrid nanofluid along with the volume fractions.
- Thermal performance factor decreases with Reynolds number, and an increase in volume fraction negatively affects the thermal performance factor.
- With the exceptions of Re = 100 and Re = 200, the wavy microchannel consistently exhibits the highest Nusselt number in all cases. In comparison to the straight microchannel, the MHD-affected straight microchannel has yielded a higher Nusselt number. Furthermore, the wavy microchannel has achieved a higher Nusselt number than the straight microchannel. This is ascribed to the combined impact of MHD and wavy surfaces, which amplify mixing and generate more significant temperature gradients within the flow.
- The wavy microchannel produces the highest pressure drop, whereas the straight microchannel generates the lowest pressure drop, these results are consistent with Nusselt number.
- Straight microchannel and straight microchannel with MHD produces similar thermal performance factors. Thermal performance factor of wavy channel is smaller than other two cases which are straight microchannel and straight microchannel with MHD

References

Ahmed, F., Fuad, M.A.A.M., Akter, F., Bhowmik, P.K., Alam, S.B. and Kumar, D. (2021) 'Numerical investigation of the thermos-hydraulic performance of water-based nanofluids in a dimpled channel flow using Al2O3, CuO, and hybrid Al2O3-CuO as nanoparticles', *Heat Transfer*, Vol. 50, No. 5, pp.5080–5105.

Aminian, E., Moghadasi, H. and Saffari, H. (2020) 'Magnetic field effects on forced convection flow of a hybrid nanofluid in a cylinder filled with porous media, a numerical study', *Journal of Thermal Analysis and Calorimetry*, Vol. 141, No. 5, pp.2019–2031.

Aminossadati, S.M, Raisi, A. and Ghasemi, B. (2021) 'Effects of magnetic field on nanofluid farced convection in a partially heated microchannel', *International Journal of Non-Linear Mechanics*, Vol. 46, No. 10, pp.1373–1382.

Ansys-Fluent (2018) *Ansys-Fluent 19.2 User's Guide*, Ansys-Inc., Canonsburg, PA.,

Asadi, A., Alarifi, I.M. and Foong, L.K. (2020) 'An experimental study on characterization stability and dynamic viscosity of CuO-TiO_2/water hybrid nanofluid', *Journal of Molecular Liquids*, Vol. 307, p.112987.

Aslan, E., Nahavandi, A., Taymaz, I. and Benim, A.C. (2012) 'A note on modelling non-rectangular boundaries by the Lattice Boltzmann method', *Progress in Computational Fluid Dynamics – An International Journal*, Vol. 12, No. 6, pp.433–438, https://doi.org/10.1504/PCFD.2012.049815.

Avci, M. (2008) *Fluid Flow and Heat Transfer in Microchannels*, PhD thesis in Karadeniz Technical Universiy (KTU)

Behroyan, I., Ganesan, P., He, S. and Sivasankaran, S. (2015) 'Turbulent forced convection of Cu-water nanofluid: CFD model comparison', *International Communications in Heat and Mass Transfer*, Vol. 67, pp.163–172.

Benim, A.C. (1990) 'Finite element analysis of confined turbulent swirling flows', *International Journal for Numerical Methods in Fluids*, Vol. 11, No. 6, pp.697–717, https://doi.org/10.1002/fld.1650110602.

Benim, A.C. and Zinser, W. (1986) 'A segregated formulation of Navier-Stokes equations with finite elements', *Computer Methods in Applied Mechanics and Engineering*, Vol. 57, No. 2, pp.223–237, https://doi.org/10.1016/0045-7825(86)90015-0.

Bhattacharyya, S., Benim, A.C., Chattopdhyay, H. and Banerjee, A. (2019) 'Experimental and numerical analysis of forced convection in a twisted tube', *Thermal Science*, Vol. 23, No. 4, pp.1043–1052, https://doi.org/10.2298/TSCI19S4043B.

Bhattacharyya, S., Benim, A.C., Pathak, M., Chamoli, S., Gupta, A. (2020) 'Thermohydraulic characteristics of inline and staggered angular cut baffle inserts in the turbulent flow regime', *Journal of Thermal Analysis and Calorimetry*, Vol. 140, pp.1519–1536, https://doi.org/10.1007/s10973-019-09094-8.

Biswas, N., Mandal, D.K., Manna, N.K. and Benim A.C. (2022) 'Magneto-hydrothermal triple-convection in a W-shaped porous cavity containing oxytactic bacteria', Vol. 12, p.18053, https://doi.org/10.1038/s41598-022-18401-7.

Cakir, M. and Aktürk, D. (2022) 'Numerical Investigation of heat transfer performance in laminar flow of nanofluids in the wavy microchannel', *Journal of Polytechnic*, Vol. 25, No. 2, pp.1769–1775.

Cengel, Y.A. and Cimbala, J.M. (2010) *Fluid Mechanics: Fundamental Applications*, McGraw-Hill Higher Education, New York.

Chen J., Ahmad, S., Deng, W., Cai, J. and Zhao, J. (2022) 'Micro/nanoscale surface on enhancing the microchannel flow boiling performance: a Lattice Boltzmann simulation', *Applied Thermal Engineering*, Vol. 205, p.118036, https://doi.org/10.1016/j.applthermaleng.2022.118036.

Chen, C., Teng, J.T., Cheng, C.H., Jin, S., Huang, S., Liu, C., Lee, M.T., Pan, H.H. and Greif, R. (2014) 'A study on fluid flow and geat transfer in rectangular microchannels with various longitudinal vortex generators', *International Journal of Heat and Mass Transfer*, Vol. 69, pp.203–214.

Ebrahimi, A., Rikhtegar, F., Sabaghab, A. and Roohi, E. (2016) 'Heat transfer and entropy generation in a microchannel with longitudinal vortex generators using nanofluids', *Energy*, Vol. 101, pp.190–201.

Ebrahimi, A., Roohi, E. and Kheradmand, S. (2015) 'Numerical study of liquid flow and heat transfer in rectangular microchannel with longitudinal vortex generators', *Applied Thermal Engineering*, Vol. 78, pp.576–583-201.

Ekiciler, R. and Çetinkaya, M.S.A. (2020) 'A comparative heat transfer study between manotype and hybrid nanofluid in a duct with various shapes of ribs', *Thermal Science and Engineering*, Vol. 23, p.100913.

Ghachem, K. Aich, W. and Kolsi, L. (2021) 'Computational analysis of hybrid nanofluid enhances heat transfer in cross flow micro heat exchanger with rectangular wavy channels', *Case Studies in Thermal Engineering*, Vol. 24, p.100822.

Goudarzi, S., Shekaramiz, M., Omidvar, A., Golab, E., Karimipour, A. and Karimipour, A. (2020) 'Nanoparticles migration due to thermophoresis and Brownian motion and its impact on Ag-MgO/Water hybrid nanofluid natural convection', *Powder Technology*, Vol. 375, pp.493–503.

Gravndyan, Q., Akbari, O.A., Toghraie, D., Marzban, A., Mashayekhi, R., Karimi, R. and Pourfattah, F. (2017) 'The effect of aspect ratios of rib on thee heat transfer and laminar water/TiO_2 nanofluid flow in a two-dimensional rectangular microchannel', *Journal of Molecular Liquids*, Vol. 236, pp.254–265.

Huminic, G. and Huminic, A. (2020) 'Entropy generation of nanofluid and hybrid nanofluid in thermal systems: a review', *Journal of Molecular Liquids*, Vol. 32, p.112533.

Khan, M.Z.U., Younis, M.Y., Akram, N., Akbar, B., Rajput, U.A., Bhutta, R.A., Uddin, E., Jamil, M.A., Garcia Marquez, F.P. and Zahid, F.B. (2021) 'Investigation heat transfer in wavy and dual wavy micro-channel heat sink alumina nanoparticles', *Case Studies in Thermal Engineering*, Vol. 28, p.101515.

Kleinstreuer, C. and Feng, Y. (2011) 'Experimental and theoretical studies of nanofluid thermal conductivity enhancement: A review', *Nanoscale Research Letters*, Vol. 6, p.229.

Krishna, V., Kumar, M.S., Mahesh, O. and Kumar, P.S. (2021) 'Numerical investigation of heat transfer and pressure drop for cooling of microchannel heat sink using MWCNT-CuO-water hybrid nanofluid with different mixture ratio', *Materials Today: Proceedings*, Vol. 42, No. 1, pp.969–974.

Kumar, V. and Sarkar, J. (2020) 'Particle ratio optimization of Al2O3-MWCNT hybrid nanofluid in minichannel heat sink for best hydrothermal performance', *Applied Thermal Engineering*, Vol. 165, p.114546.

Kuppan, T. (2000) *Heat Exchanger Design Handbook*, Dekker Inc, New York.

Ma, Y., Modebbi, R., Rashidi, M.M. and Yang, Z. (2019) 'MHD convective heat transfer of Ag-MgO/water hybrid nanofluid in a channel with active heaters and coolers', *International Journal of Heat and Mass Transfer*, Vol. 137, pp.714–726.

Manay, E., Sahin, B., Akyurek, F.E. and Comakli, O. (2012) 'The use of nanofluids in microchannels', *Engineer and Machine*, Vol. 627, No. 53, pp.39–42.

Nguyen, Q., Bahrami, D., Kalbasi, R. and Bach, Q.V. (2020) 'Nanofluid flow through microchannel with a triangular corrugated wall: heat transfer enhancement against entropy generation intensification', *Mathematical Methods in Applied Sciences*, pp.1–14.

Okhotin, A., Pushkarskii, A. and Gorbachev V. (1972) *Thermophysical properties of semiconductors*, Atom Publishing House, Moscow.

Salman, S., Saadon, A.A. and Sultan, M.H. (2020) 'Hybrid nanofluid flow and heat transfer over backward and forward steps: a review', *Powder Technology*, Vol. 363, No. 1, pp.448–472.

Selimefendigil, F. and Öztop, H.F. (2023) 'Thermal and phase change process in a branching T-channel under active magnetic field and two rotating inner cylinders: analysis and predictions by radial basis neural networks', *International Journal of Heat and Mass Transfer*, Vol. 217, p.124548.

Selimefendigil, F., Öztop, H.F. and Al-Salem, K. (2014) 'Natural convection of ferrofluids in partially heated square enclosures', *Journal of Magnetism and Magnetic Materials*, Vol. 372, pp.122–13v3.

Sheikholeslami, M., Abelman, S. and Ganji, D.D. (2014) 'Numerical simulation of MHD nanofluid flow and heat transfer considering viscous dissipation', *International Journal of Heat and Mass Transfer*, Vol. 79, pp.212–222.

Shiriny, A., Bayareh, M., Nadooshan, A.A. and Bahrami, D. (2019) 'Forced convection heat transfer of water/FMWCNT nanofluid in a microchannel with triangular ribs', *SN Applied Sciences*, Vol. 1, p.1631.

Sivasankaran, S. and Narrein, K. (2020) 'Influence of geometry ad magnetic field on convective flow of nanofluids in trapezoidal microchannel heat sink', *Iranian Journal of Science and Technology, Transactions of Mechanical Engineering*, Vol. 44, No. 2, pp.373–382.

Soltanipour, H., Khalilarya, Motlagh, S.Y. and Mirzaee, I. (2017) 'The effect of position-dependent magnetic field on nanofluid forced convective heat transfer and entropy generation in a microchannel', *Journal of Brazilian Society of Mechanical Sciences and Engineering*, Vol. 39, No. 1, pp.345–355.

Tawfik, M.M. (2017) 'Experimental studies of nanofluid thermal conductivity enhancement and applications: a review', *Renewable and Sustainable Energy Reviewers*, Vol. 75, pp.1239–1253.

Vajjhai, R.S., Das, D.K. and Kulkarni, D.P. (2010) 'Development of new correlations for convective heat transfer and friction factor in turbulent regime for nanofluids', *International Journal of Heat and Mass Transfer*, Vol. 53, Nos. 21–22, pp.4607–4618.

Vinoth, R. and Sachuthananthan B. (2021) 'Flow and heat transfer behavior of hybrid nanofluid through microchannel with two different channels', *International Communications in Heat and Mass Transfer*, Vol. 123, p.105194.

Xia, J. L., Smith, B. L., Benim, A. C., Schmidli, J., Yadigaroglu, G. (1997) 'Effect of inlet and outlet boundary conditions on swirling flows', *Computers and Fluids*, Vol. 26, No. 8, pp.811–823, https://doi.org/10.1016/S0045-7930(97)00026-1.

Yu, W. and Choi, S.U.S. (2003) 'The role of interfacial layers in the enhances thermal conductivity of nanofluids: a renovated Maxwell model', *Journal of Nanoparticle Research*, Vol. 5, No. 1, pp.167–171.